Simulation of Spaced Antenna Wind Retrieval Performance on an X-Band Active Phased Array Weather Radar

V. VENKATESH AND S. J. FRASIER

Microwave Remote Sensing Laboratory, University of Massachusetts–Amherst, Amherst, Massachusetts

ABSTRACT

Spaced antenna baseline wind retrievals, in conjunction with traditional Doppler measurements, are a potential means of fine angular resolution weather radar wind vector retrieval. A spaced antenna implementation on an X-band active phased array architecture is investigated via Monte Carlo simulations of the backscattered electric fields at the antenna array. Several retrieval methods are exercised on the data produced by the simulator. Parameters of the X-band spaced-antenna design are then optimized. Benefiting from the parametric fitting procedure inherent in the time domain slope at zero lag and full correlation analysis, the study finds both of these algorithms to be more immune to thermal noise than the spectral retrieval algorithms investigated. With appropriately chosen baselines, these time domain algorithms are shown to perform adequately for 5-dB SNR and above. The study also shows that the Gaussian slope at zero lag (G-SZL) algorithm leads to more robust estimates over a wider range of beamwidths than the Gaussian full correlation analysis (G-FCA) algorithm. The predicted performance of the X-band array is compared to a similar spaced antenna implementation on the S-band National Weather Radar Testbed (NWRT). Since the X-band signal decorrelates more rapidly (relative to S band), the X-band array accumulates more independent samples, thereby obtaining lower retrieval uncertainty. However, the same rapid decorrelation also limits the maximum range of the X-band array, as the pulse rate must be sufficiently high to sample the cross-correlation function. It also limits the range of tolerable turbulence velocity within the resolution cell.

1. Introduction

Over the past several decades, single-Doppler radar wind field retrieval techniques that rely on the scanning capabilities of weather radars have been developed. One such method, the velocity–azimuth display (VAD), obtains the wind vector from the best fit to azimuthal harmonics of radial velocity data (Probert-Jones 1960; Lhermitte and Atlas 1961). Although advances in this family of methods continue to be made (Caya and Zawadski 1992), their application implicitly assumes that the large-scale kinematics of the wind field are spatially continuous. Here, large is relative to the dimensions of a single-resolution volume. Another such method originally retrieved the wind vector by tracking reflectivity centroids (Rinehart and Garvey 1978) and is referred to as the tracking of reflectivity echoes by correlation (TREC). In spite of the continued advances in the centroid tracking

family of techniques (Smythe and Zrnic 1983), their use has been shown to be limited to scenarios of dominant horizontal advection (Kramar et al. 2005).

Methods that rely on the scanning capability of weather radars to retrieve the wind field invariably sacrifice angular resolution to do so. For the VAD family, this is implicit in the fit across the azimuthal dimension of data. For the TREC family, this is because of the need to estimate the centroid that is ultimately tracked. Yet another method based on simulated predictions of motion, the variational method, has also been reported to quantitatively favor coarse angular-resolution retrievals (Shapiro et al. 2006).

For ionospheric and boundary layer profiling applications, the spaced antenna (SA) method has been routinely used for single-radar-based crossbeam wind retrieval in addition to the traditional Doppler (radial) component of velocity. The SA method employs two copointed antennas separated by a small distance and estimates the component of wind along the direction of separation (i.e., the antenna baseline) by correlating the backscattered electric fields received by the two apertures. A related

and generally less favorable SA implementation that uses angularly displaced resolution volumes, now referred to as angular interferometry (Zhang et al. 2003a), has also been applied for lidar profiling (Sroga et al. 1980). The application of the SA method, if proven practical for weather radars, is a potential means of single-radar-based high-angular-resolution wind vector retrieval.

In this work, we investigate SA baseline wind retrieval on a candidate X-band active phased array (Salazar et al. 2008) based on Monte Carlo simulations of scatterer advection by spatially homogeneous mean wind and turbulence velocity. The following section presents our approach to SA aperture synthesis, our simulation methodology, and retrieval algorithms that we consider for investigation with numerical simulations. We then investigate SA baseline wind retrieval at X band by analyzing its sensitivity to rms turbulence velocity and thermal noise.

2. Methodology

a. Considerations for SA weather radar

Spaced antenna concepts have been reviewed in several works (Briggs et al. 1950; Briggs 1985; Larsen and Röttger 1989; Doviak et al. 1996; Holloway et al. 1997; Zhang and Doviak 2007), and can be explained through the cross-correlation function of backscattered electric fields sampled by two monostatic antenna systems A_1 and A_2 separated by a baseline Δx. For SA wind estimation, the idea is that the advection of scatterers parallel to the SA baseline causes the observed signals to fade. In the presence of strictly laminar along-baseline wind, the time series at receiver A_2 is exactly the same as that received at A_1 except delayed by a time lag, $\tau = \Delta x / v_x$. This is the time taken for the scatterers in the resolution volume of A_1 to advect to that of A_2 (Zhang and Doviak 2007; Doviak et al. 1996; Zhang et al. 2003b). Although the basic idea is simple, the simultaneous rearrangement of scatterers by other components of the wind field and by turbulence results in a change in the apparent delay that must be corrected. Effectively, SA wind estimation is based on a model of the expected correlation function given by

$$|\langle\gamma(\Delta x, \tau)\rangle| = \exp[-2k^2\sigma_\phi^2(v_x\tau - \Delta x)^2]$$
$$\times \exp(-2k^2\sigma_\theta^2 v_y^2\tau^2)\exp(-2k^2\sigma_{tz}^2\tau^2), \quad (1)$$

where k is the radar wavenumber; Δx is the spaced antenna baseline; σ_{tz} is the rms radial velocity due to turbulence velocity; v_x and v_y are the respective along- and cross-baseline components of velocity; and σ_ϕ and σ_θ are

the square root of the second central moment of the two-way azimuthal and elevational antenna pattern, respectively. The expression in (1) is derived from Doviak et al. (1996) and Holloway et al. (1997) for the special case of point scatterers. It may also be obtained from Zhang and Doviak [2007, their Eq. (13)] for the case of zero shear in the radial wind. The relationship between the second central moment of the two-way antenna pattern, σ_ϕ^2, and a one-way half-power beamwidth, ϕ_1, is $\sigma_\phi^2 = \phi_1^2/16\ln2$. In the case where different sized antennas are used for transmission and reception, an effective one-way beamwidth can be defined in terms of the beamwidths of the transmitting and receiving antennas, $\phi_1 = \sqrt{2}[\sqrt{(1/\phi_{1T}^2) + (1/\phi_R^2)}]^{-1}$. Here, ϕ_{1T} and ϕ_{1R} denote the half-power beamwidths of the transmit and receive antenna patterns, respectively. Since manufacturers typically specify antenna systems with one-way 3-dB antenna beamwidths, we have chosen the same metric for design specification. Hence, we slightly differ in notation from Zhang and Doviak (2007), who instead use two-way beamwidths.

The expression in (1) is the product of three Gaussian terms. The first describes the effect of the along-baseline wind on the correlation and is of primary interest. The second term describes the effect of cross-baseline winds. Small cross-baseline beamwidths reduce its impact. Together, these first two terms describe the effect of mean wind traversing a finite beamwidth antenna pattern and we denote this beam broadening decorrelation. The third term in (1) describes the effect of turbulence velocity on the correlation function, and it depends upon the rms radial motion of the scatterers.

The terms of (1) are illustrated in Fig. 1. Here, the solid curve represents the first term, and the dotted curve represents the product of the second and third terms (denoted as γ_{turb}). Note, in this case the cross-baseline wind is set to zero. The dashed line is the product of all the terms, which is also a Gaussian, but reduced in amplitude and shifted toward zero lag. The objective of SA retrieval is to account for the deleterious effects of the second and third Gaussian terms. As a practical matter, the peak of the observed cross correlation needs to be sufficiently high to allow for its estimation (Larsen and Röttger 1989).

Since the impact of turbulence velocity is large at X band, short baselines are needed to mitigate turbulent decorrelation. The required baseline is often significantly less than the antenna aperture size, and thus in practice the two antenna apertures must physically overlap. Schemes to implement such an aperture include the dual-polarization spaced antenna described by Pazmany et al. (2004) and Hardwick et al. (2005). This approach resulted in a fixed spacing with little means for adjustment, and
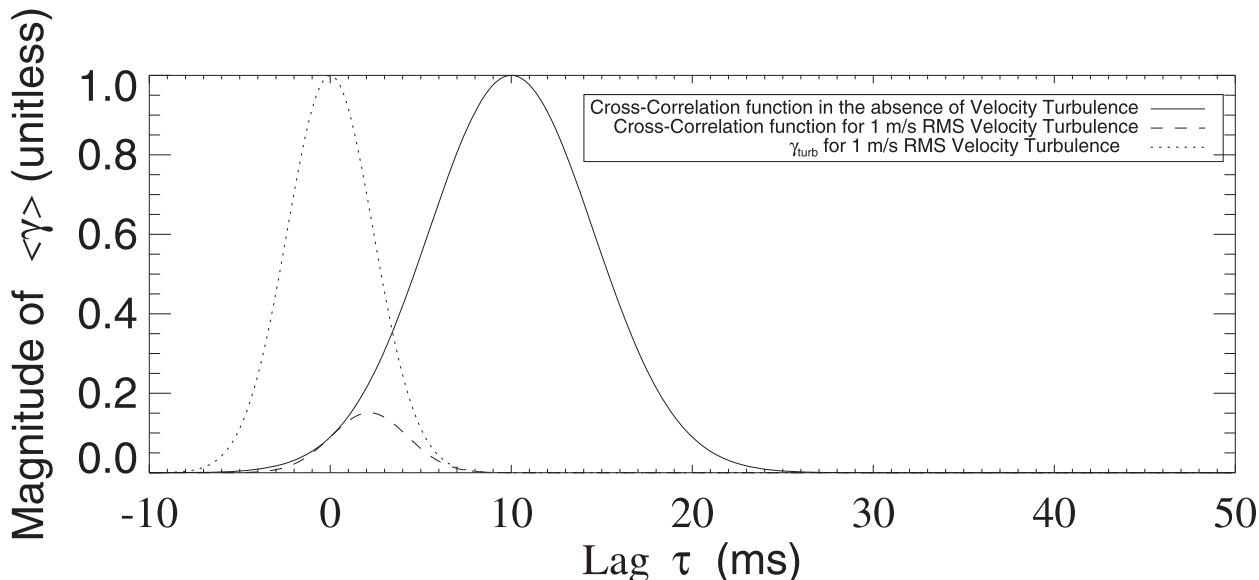
FIG. 1. Decomposition of the expected cross-correlation function for $1\,\mathrm{m\,s^{-1}}$ rms turbulence velocity in the absence of cross-baseline wind. Parameters are $\lambda = 3\,\mathrm{cm}$, equivalent one-way antenna azimuthal 3-dB beamwidth $\phi_1 = 4°$, $\Delta x = 25\,\mathrm{cm}$, $v_x = 25\,\mathrm{m\,s^{-1}}$, and $v_y = 0\,\mathrm{m\,s^{-1}}$.

relied upon the separable yet well-correlated scattering of orthogonal polarization by hydrometeors.

The measurement of crossbeam velocity is further confounded by mechanical slewing of the antenna that results in the horizontal translation of the sampling volume during measurement. The resulting effective horizontal velocity easily overwhelms the desired measurement at moderate ranges. These limitations, however, can be overcome with the use of an active phased array aperture.

The University of Massachusetts is developing a planar active phased array antenna system that is capable of electronic scanning in azimuth and mechanical actuation in elevation (Salazar et al. 2008). It consists of a 64-element array of fan-beam antenna elements. Behind each element, a transmit–receive module provides programmable amplitude weighting on transmit and receive. Figure 2 depicts an approach to implementing overlapped spaced apertures using this phased array antenna system.

The entire array aperture is used upon transmission, while alternating portions of the array are used upon reception. Auto- and cross correlations may be produced with the interleaved time series from the subarrays. The effective phase centers of the overlapped apertures are located midway between the centers of the transmit and receive apertures. Therefore, with this implementation, the effective SA baseline is half the physical distance between the centers of the "left" and "right" receive apertures. This is similar to the scheme employed by the Multiple Antenna Profiler (MAPR) UHF radar (Cohn et al. 1997, 2001) and to that described using the National Weather Radar Testbed (NWRT) S-band radar (Zhang and Doviak 2007). The primary strength of the active phased array system is in the ability to synthesize various SA baselines and effective aperture sizes through the programmable amplitude weighting on transmit and receive. Furthermore, because phased arrays are able to "step scan,"
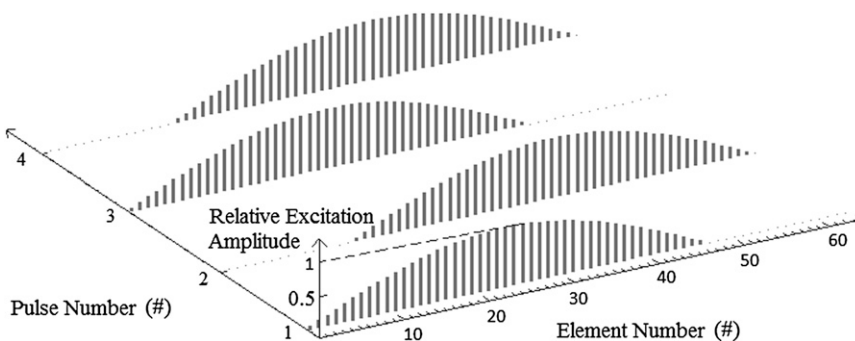

FIG. 2. Time series of transmit–receive aperture weighting with alternating left and right receive apertures. During transmit, the phase center of the aperture is at its physical center.

dwelling on successive azimuth locations with near-instantaneous switching in between, the problems associated with the apparent translational velocity due to mechanical scanning are avoided.

b. Algorithms for SA baseline wind retrieval

1) TIME DOMAIN METHODS

With spaced aperture correlation functions or cross-spectral estimates, a variety of algorithms are available to correct for the effect of turbulence velocity based on inversions of the forward model. Equation (1) can be expressed as (Holloway et al. 1997)

$$|\langle \gamma(\Delta x, \tau) \rangle| = \exp(-\eta) \exp\left[-\frac{(\tau - \tau_p)^2}{2\tau_c^2}\right], \qquad (2)$$

where the parameters η, τ_p, and τ_c describe the amplitude, time lag, and width of the observed cross correlation, respectively. These observables can be related back to the desired parameters, v_x, v_y, and σ_{tz}. Doviak et al. (2004) compare time domain algorithms and conclude that the implementation of the full correlation analysis that assumes Gaussian forms for the correlation functions (G-FCA) and slope at zero lag (G-SZL) implementations are the best time domain algorithms in the absence of thermal noise. In Doviak et al. (2004), frequency domain SA baseline wind estimation was not considered. Here, frequency domain equivalents of these algorithms are included for investigation with numerical simulations.

In the G-FCA approach, the along-baseline wind is retrieved using (Holloway et al. 1997)

$$\hat{v}_{xG\text{-FCA}} = \Delta x \frac{\hat{\tau}_p}{2\hat{\eta}\hat{\tau}_c^2 + \hat{\tau}_p^2} \qquad (3)$$

and the standard deviation (SD) of the estimate is given approximately by (Doviak et al. 2004).

$$\text{SD}(\hat{v}_{xG\text{-FCA}}) = \frac{\hat{v}_x}{2(1+p^2)\sqrt{N}}$$
$$\times \sqrt{3 + \frac{(1-p^2)(e^{2\eta}-1)}{2\eta p^2} + \frac{4(\cosh 2\eta - 1)}{\eta^2}},$$
$$(4)$$

where $N = T_d/\pi\tau_c$, $p = v_s/v_x$, and T_d is the dwell time of the measurement(s).

An alternative way of estimating $\hat{v}_x$ is by direct elimination of the effective decorrelating wind (denoted as v_s in the appendix) (Lataitis et al. 1995; Zhang et al. 2003a). One such algorithm that uses this elimination is the SZL method, given by (Lataitis et al. 1995)

$$\hat{v}_{xSZL} = \frac{1}{4k^2\sigma_\phi^2 \Delta x} M, \qquad (5)$$

where $M(\tau = 0)$ is the normalized slope of the cross-correlation function evaluated at zero temporal lag:

$$M = \frac{d}{d\tau}\left[\frac{\gamma(\Delta x, \tau)}{\gamma(\Delta x, 0)}\right]\bigg|_{\tau=0}. \qquad (6)$$

A common implementation to estimate M is a finite difference approximation to the slope of the cross-correlation function at zero lag. The application of this implementation for X-band radars is, however, impractical, as the precise zero-lag slope of the cross correlation cannot be easily estimated given typical pulse repetition rates. For this reason, we use an alternate implementation that relies on the functional form of the correlation (see the appendix) where τ_p/τ_c^2 is mathematically equivalent to M (Doviak et al. 2004). Thus, the SA baseline wind is explicitly retrieved using

$$\hat{v}_{xG\text{-SZL}} = \frac{1}{4k^2\sigma_\phi^2 \Delta x} \frac{\tau_p}{\tau_c^2} \qquad (7)$$

and its standard deviation for long dwell times is given by (Doviak et al. 2004)

$$\text{SD}(\hat{v}_{xG\text{-SZL}}) = \frac{\hat{v}_x}{\sqrt{N}} \sqrt{\frac{3}{4} + \frac{1 - e^{-2\eta}}{4e^{-2\eta}}}. \qquad (8)$$

Another way to estimate the normalized slope at zero lag is to invoke the moments theorem (Muschinski 2004) and to retrieve the wind speed from the ratio of first to zeroth cross-spectral moments. Specifically, the moments theorem ties the complex phase moments of the cross spectra to the derivatives of the cross-correlation function

$$I^m = \frac{d^m}{d\tau^m}\gamma(\Delta x, \tau = 0) = \int (j\omega)^m S(\Delta x, \omega), \qquad (9)$$

where $S(\Delta x, \omega)$ is the cross spectrum of the back-scattered electric fields. The explicit functional form of this retrieval is given by

$$\hat{v}_{xD\text{-SZL}} = \frac{1}{4k^2\sigma_\phi^2 \Delta x} \frac{\hat{I}^1}{\hat{I}^0}, \qquad (10)$$

where I^0 and I^1 are the zeroth and first cross-spectral moments, respectively. It can be shown that this implementation does not require the assumption of a Gaussian function form, and hence the subscript D for direct.
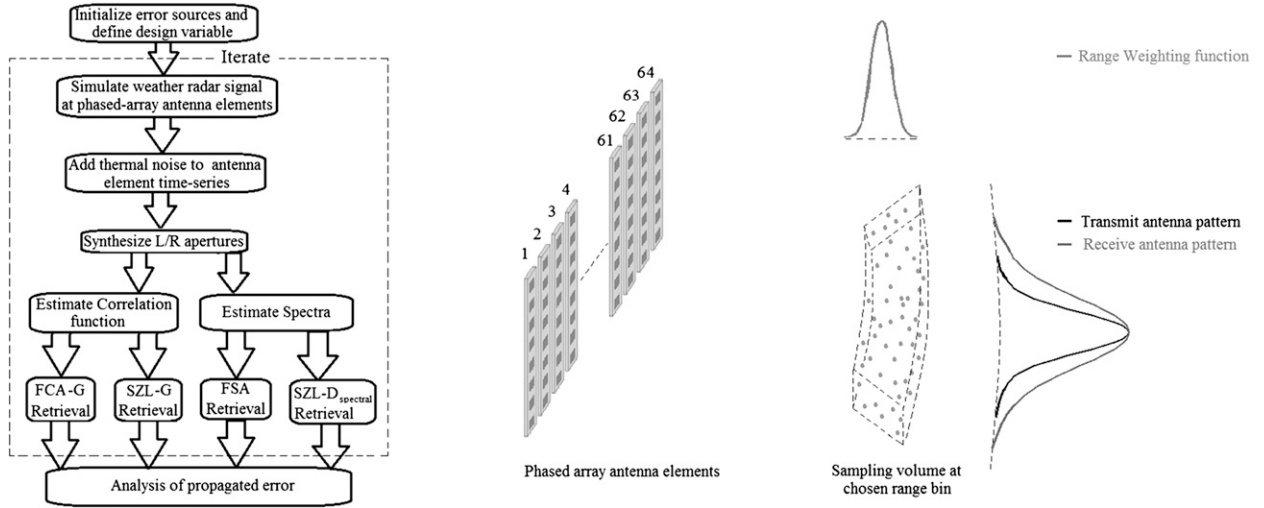
FIG. 3. (left to right) Illustration of algorithm used to study performance of a phased array spaced antenna system, sampling volume, and conceptual range weighting function and antenna patterns of the phased array weather radar signal simulator.

2) SPECTRAL METHODS

The full spectral analysis (FSA) method comes from the mesosphere–stratosphere–troposphere (MST) radar community (Briggs and Vincent 1992), where the source of scattering is almost always inhomogeneous (e.g., local plasma irregularities or ionized meteor trails). In other words, when the anticipated beam filling is nonuniform and/or bimodal spectra are observed, spectral analysis methods have been employed. Its equivalence to the G-SZL is apparent in the appendix. However, it is not obvious at this point as to how the error of SA baseline wind estimation in the frequency domain compares to other implementations of the G-SZL. We note that Kudeki and Sürücü (1991), Briggs and Vincent (1992), and Holdsworth and Reid (1995b) call their frequency domain methods by the same name without correcting for turbulence velocity, and only use the autospectrum to estimate the horizontal correlation length of the Bragg scatterers. The explicit functional form for FSA retrieval we use is given by (Holloway et al. 1997)

$$\hat{v}_{x\mathrm{FSA}} = \frac{1}{4k^2\sigma_\phi^2\Delta x}\frac{\hat{m}\hat{\sigma}_w^2}{2k},$$ (11)

where $\hat{m}$ is the slope of the cross-spectral phase in the Doppler velocity domain,

$$m = \frac{d}{dv}\arg S(\Delta x, v),$$ (12)

and $\hat{\sigma}_w$ is the Doppler spectrum width. Here, $\hat{m}$ is estimated by a linear fit to the signal containing part of the cross-spectral phase and, based on the Fourier shift

theorem, is essentially an estimate of the lag to cross-correlation peak. The symbol $\hat{\sigma}_w$ is estimated by fitting a Gaussian to the smoothed Doppler spectrum and it corrects the retrieval for turbulence velocity and cross-baseline wind. Although $\hat{\sigma}_w$ can also be estimated from the cross spectrum, we use the autospectrum width estimate, as we expect that it has a variance lesser than or equal to the cross spectrum, analogous to the time domain case (Doviak et al. 2004).

c. Simulation of an active phased array SA weather radar

Our approach to numerical simulations is to estimate correlation coefficients from simulated backscattered electric fields at spaced antennas using a weather radar simulator capable of generating two-dimensional (time and azimuth) data, similar to that described in Cheong and Palmer (2008) and Holdsworth and Reid (1995a). The general structure of the simulation algorithm we use for our study is depicted in Fig. 3. To initialize the simulator, the complex excitation coefficients of the phased array antenna system and radar, and the meteorological parameters are prescribed. From these values, an enclosing volume centered on the illuminated footprint is defined. The dimensions of the initialized resolution volume are dictated by the smallest receive aperture we wish to investigate for spaced antenna aperture synthesis and by the range resolution. This choice of the azimuthal dimension of the bounding volume is, solely, to provide convenient run times for the simulation.

The bounding volume is populated with N_s randomly placed point scatterers and the received voltage of the jth antenna element (proportional to the electric field) is given by

$$V_j(t) = \sum_{n=1}^{N_s} A_{j,n} R_n \exp[-ik(r_n + r_{j,n})], \qquad (13)$$

where $A_{j,n}$ is the antenna weighting function of the antenna element j, R_n is the range weighting function, r_n is the distance between the transmitter and the nth scatterer (common to all elements), and $r_{j,n}$ is the range to the receiving element. The antenna weighting functions used to mimic a volume scattering scenario is given by (Doviak and Zrnić 1993; Zhang and Doviak 2007).

$$A_{j,n} = \exp\left[-\frac{(X_0 - X_n)^2}{4r_0^2\sigma_{\phi 1T}^2} - \frac{(X_j - X_n)^2}{4r_0^2\sigma_{\phi elem}^2} - \frac{(Y_0 - Y_n)^2}{2r_0^2\sigma_\theta^2}\right],$$
$$(14)$$

where $\sigma_{\phi 1T}$ and $\sigma_{\phi elem}$ are the second central moment of azimuthal transmit and element antenna patterns, respectively; and σ_θ is the second central moment of the effective two-way elevational antenna pattern. The range weighting function and its relationship to transmitted chirp bandwidth is given by (Doviak and Zrnić 1993)

$$R_n = \exp\left[-\frac{(Z_0 - Z_n)^2}{2\sigma_R^2}\right], \qquad (15)$$

$$\sigma_R = 0.35\frac{c}{2B}, \qquad (16)$$

where c is the speed of light ($m\,s^{-1}$) and B is the transmitted chirp bandwidth. The constant 0.35 approximately accounts for losses due to amplitude modulation of the chirp and finite receiver bandwidth.

Scatterer locations are updated at every pulse repetition interval, given mean and turbulent velocity components along each coordinate. Gaussian-distributed pseudorandom values are used to generate the turbulent velocity fields. Since the omission of temporal continuity of the turbulence velocity causes individual scatterers to have abrupt changes in the turbulent velocity (Holdsworth and Reid 1995a), we run a five-point moving average filter to low-pass filter the turbulent velocity in the temporal dimension as described by Cheong and Palmer (2008). It is this low-pass filtering by the moving average filter that distinguishes turbulence velocity from random Brownian motion and from random changes in the phase of the composite signal introduced by thermal noise.

Once the time and azimuthal series data are generated at each element, thermal noise is added directly to each element. Finally, the time series data are summed across several antenna elements and are used to provide time series samples of each aperture. Correlation functions and cross spectra are then estimated from the time series

TABLE 1. Nominal simulation parameters.

Parameter	Value
Radar center frequency	9.6 GHz
PRF	5 kHz
Phased array element spacing	1.6 cm
Number of available elements	64
Equivalent one-way antenna azimuthal 3-dB beamwidth	3°
Effective spaced antenna baseline	4.5 cm
Dwell time	2 s
Range to resolution volume	10 km
Number of scatterers	300
SA baseline wind speed	$10\,m\,s^{-1}$
Cross-baseline wind speed	$0\,m\,s^{-1}$
Radial (Doppler) velocity	$10\,m\,s^{-1}$
RMS velocity turbulence	$2\,m\,s^{-1}$
SNR	10 dB

using alternate samples to mimic interleaving, illustrated in Fig. 2. Typically, 100 trials are performed in order to produce the statistics of the next section.

3. Results

a. Design of an X-band spaced antenna weather radar

Here, the design space of an X-band spaced antenna is investigated by studying the sensitivity to retrieval errors propagated from turbulence velocity and thermal noise. To investigate the potential use of X-band spaced antenna implementations on flexible active phased array architectures, the degrees of freedom considered in the following subsections are the radar pulse repetition frequency (PRF), the spaced antenna baseline separation, and the spaced antenna aperture size. The nominal simulation parameters used are outlined in Table 1. These are the values used for each parameter when it is not being varied.

1) PRF

We desire the cross-correlation functions to be well sampled in order to accurately estimate the cross-correlation peak. This must be balanced against range ambiguity considerations. Figure 4a shows the uncertainty in the estimate of the delay to the cross-correlation peak $\hat{\tau}_p$ for the given parameters as a function of the pulse repetition frequency (i.e., temporal sampling) employed. Figure 4 shows that the standard deviation of baseline wind estimates also increases with decreasing PRF irrespective of the retrieval algorithm employed. This increase in estimation error is a direct consequence of increasing errors in the precise estimation of $\hat{\tau}_p$. Note that the increased sensitivity of the FSA to the sampling frequency is specific to the implementation of the algorithm considered here, where the cross-spectral power was
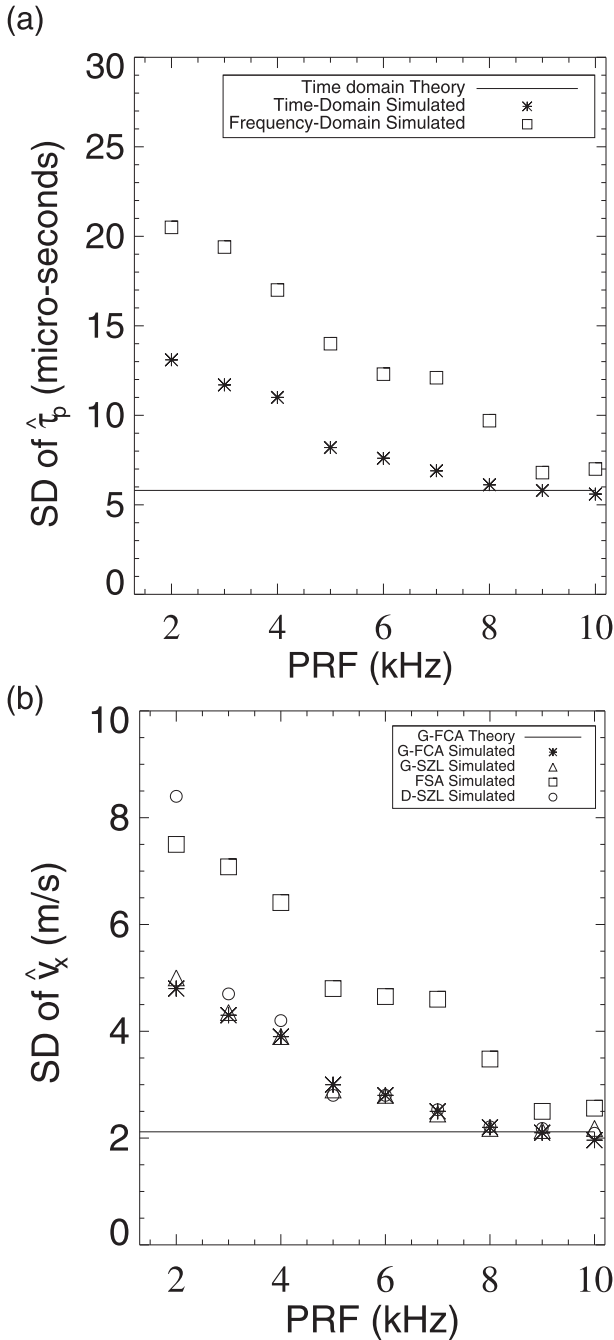
(a)

(b)

FIG. 4. Standard deviation of (a) estimated delay to the cross-correlation peak τ_p, and (b) retrieved SA baseline wind vs PRF. Simulation parameters as in Table 1 and with infinite SNR.

thresholded at 15 dB below the unsmoothed peak. Further, for all algorithms except the FSA, we observe the steepest improvement in the estimate for a PRF of 5 kHz. This pulse rate corresponds to an unambiguous range of 30 km, which is not large by weather radar standards. Improving unambiguous range would appear to require accepting greater uncertainty in SA retrievals, or

implementing other means to deal with multiple trip echoes that become problematic at high pulse rates. The choice of PRF here is suitable for the relatively small short-to-medium-range radar investigated here. It would not be suitable for a long-range system.

2) BASELINE

The two antenna apertures must be sufficiently spaced to afford a reasonable estimate of the wind in the presence of noise. They must, however, simultaneously be sufficiently close to mitigate the impact of turbulent decorrelation. Figure 5 compares the standard deviation of SZL implementations with the G-FCA method. Note that the standard deviation of the SA baseline wind estimates basically follows the same shape as the theoretical prediction. The elevated error in simulated results is attributed primarily to the finite sampling rate (i.e., the PRF).

First, we note that the G-SZL and G-FCA implementations have better immunity to thermal noise than the D-SZL implementation where the D is frequency domain. The better performance of these time domain algorithms compared to D-SZL is a direct consequence of the parametric fit to the cross-correlation function. Although the immunity of time domain estimation of has been reported in Zhang et al. (2004), to the best of our knowledge a comparison with spectral SA retrieval algorithms has not been reported to date. The inferior performance of the FSA algorithm stems from more uncertainty in estimation of $\hat{\tau}_p$, as shown in Fig. 4b. Therefore, in the rest of this work, we only consider time domain retrievals and obviate the need to optimize spectral implementations.

Second, the G-FCA retrievals require noise correction for reduced cross-correlation coefficient values but the SZL retrievals do not. The performances of the noise-corrected G-FCA and SZL without noise correction are nearly identical. Therefore, G-SZL algorithms lend to simpler implementation with little penalty in the retrieval uncertainty.

Third, we see that there is little benefit in designing the system for a signal-to-noise ratio (SNR) $\geq$ 5 dB. From the 10- and 5-dB SNR curves, we see that if the baseline is shorter than 7.5 cm, then the G-FCA and G-SZL algorithms become sensitive to thermal noise. Baselines longer than 14 cm tend to increase the retrieval error because of lower correlation coefficient magnitudes. Within this range of 7.5–12-cm baselines, there is little penalty incurred for $2 \, \mathrm{m \, s^{-1}}$ rms turbulence velocity and SNR $\geq$ 5 dB. For scanning phased array spaced antenna implementations, the baseline is a geometric projection of the physical antenna separation. Specifically, $\Delta x = \Delta x_{\mathrm{broadside}}(\cos\beta)$, where $\Delta x_{\mathrm{broadside}}$ is the baseline at broadside and β is the scan angle off broadside. We choose to fix the antenna phase center separation to 12 cm.
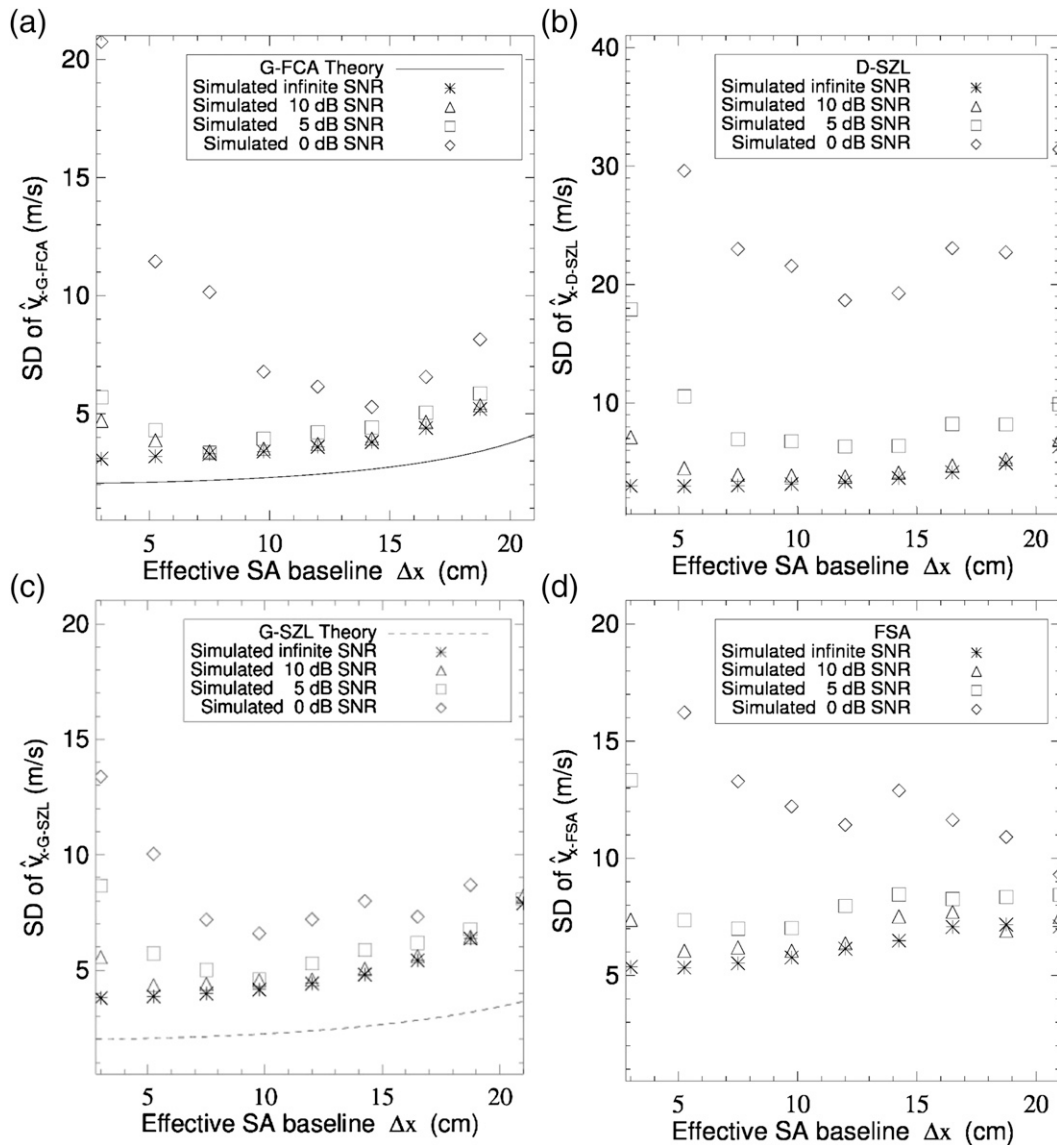
FIG. 5. Standard deviation of retrieved SA baseline wind vs effective baseline separation for various SNRs: (a) G-FCA, (b) D-SZL, (c) G-SZL, and (d) FSA. Simulation parameters as in Table 1.

For the 45° off broadside that our phased array system is capable of scanning, the baseline spans 8.4–12 cm.

3) APERTURE SIZE

Beam broadening decorrelation, upon which SA retrieval relies, favors larger beamwidths. However, narrow beams are desired for fine spatial resolution. Figure 6 shows the estimated standard deviation of the SA baseline wind estimate as a function of the effective one-way antenna beamwidth. The range of one-way antenna beamwidths simulated is representative of designs we can synthesize with the phased array antenna system. We have implemented these beamwidths by appropriate tapering of the aperture illumination as opposed to simply

using fewer elements on transmit because of the accompanying sidelobe suppression.

From Fig. 6a, we note that the design curves have regions of negative and positive slope. The negative slope is because increased sensitivity to beam broadening decorrelation from along-baseline wind leads to better estimation of $\hat{\tau}_p$. Specifically, for narrow beamwidths at X band and typical observed values of turbulence velocity, an approximate relationship for X-band weather radars is $\langle \tau_p \rangle \propto \phi_1^2 v_x$. Larger beamwidths therefore improve the sensitivity of $\langle \tau_p \rangle$ to baseline wind beamwidth in spite of the reduced available SNR at the aperture. The positive slope is a direct consequence of low correlation coefficient magnitudes impacting the estimation of $\hat{\tau}_p$ and $\hat{\eta}$.
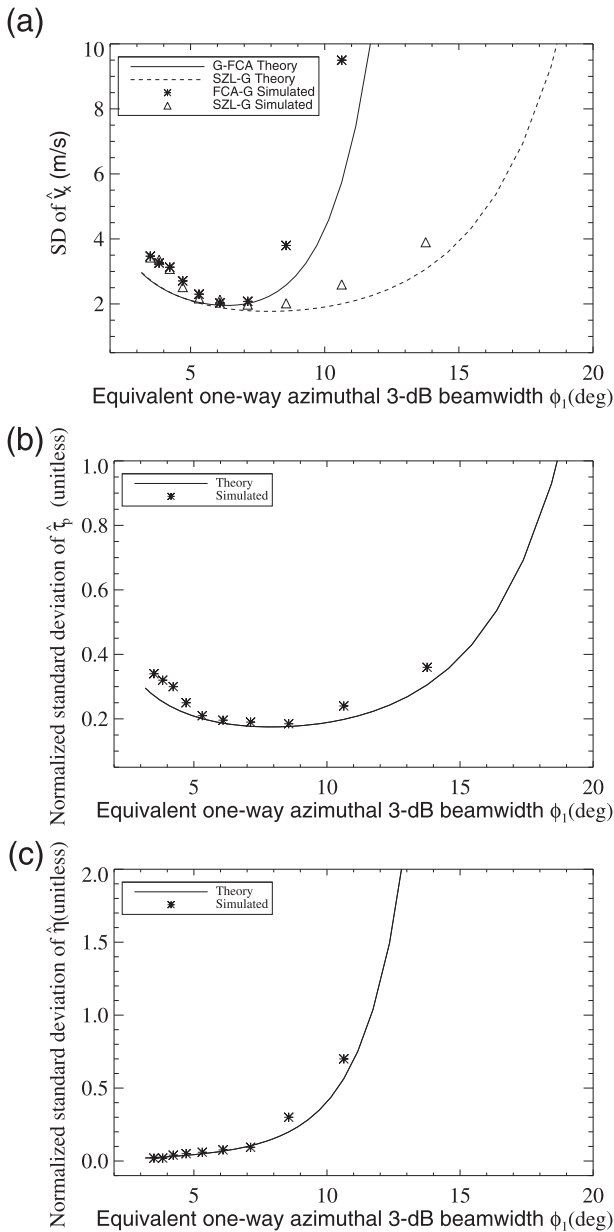
FIG. 6. (a) Standard deviation (SD) of G-SZL- and G-FCA-retrieved SA baseline wind, and normalized SD of (c) and $\hat{\eta}$ vs equivalent one-way antenna azimuthal 3-dB beamwidth for $2 \, \mathrm{m \, s^{-1}}$ rms velocity turbulence. Effective spaced antenna baseline $\Delta x = 12 \, \mathrm{cm}$, the SNR available across the entire receive array is 10 dB, and the rest of simulation parameters as in Table 1.

The value of this positive slope and the beamwidth where it begins to have an effect is coupled with the chosen baseline. From Fig. 6b, we see that the G-SZL retrieval uncertainty basically follows the same shape as the error in estimating $\hat{\tau}_p$. For beamwidths larger than 7°, the higher retrieval uncertainties in the G-FCA algorithm stem from the additional need to estimate $\hat{\eta}$ as shown in Fig. 6c. For the chosen spaced antenna baseline and rms turbulence

velocity, we see that there is little penalty in the G-SZL retrievals for one-way antenna azimuthal 3-dB beam-widths greater than 5°. Therefore, we deem a beamwidth of 5° sufficient at broadside for a 12-cm baseline and $2 \, \mathrm{m \, s^{-1}}$ rms turbulence velocity. Given that our phased array is capable of scanning up to ±45°, the corresponding one-way antenna 3-dB beamwidths lie between 5° and 7.07°. Since the effective baselines only decrease with scanning, this does not adversely impact the retrievals.

b. Performance evaluation

Figure 7 shows a comparison of the design developed in this study with the simulated performance of the NWRT (taken from Li et al. 2009) for matched wind speeds, rms velocity turbulence, dwell times, and SNR. Here, T_d is the dwell time of the measurement. First, the performance of the X-band design spans regions where the correlation function is adequately sampled and regions where it is not. For rms turbulence velocity $\leq 2 \, \mathrm{m \, s^{-1}}$, the correlation function is sufficiently sampled and the simulations closely follow theory. For rms turbulence velocity $\geq 2 \, \mathrm{m \, s^{-1}}$, the error in estimation of $\hat{\tau}_p$ due to insufficiently sampled correlation functions increases nearly exponentially and ultimately dominates the retrieval error (similar to Fig. 4b). The effect of sampling on the retrieval uncertainty is not captured in the theoretical curves. Based on these simulation results, the performance of the final design holds promise for low to moderate values of turbulence velocity typically observed with weather radars ($\leq 2 \, \mathrm{m \, s^{-1}}$).

Second, we see that for rms turbulence velocity $< 3 \, \mathrm{m \, s^{-1}}$ (typical median values in winter storms, stratiform precipitation, and scattering from biota), the designed X-band SA systems outperform the S-band SA implementation on the NWRT. Note that it has been shown that the standard deviation of the cross-correlation ratio (CCR) method is identical to that of G-SZL, for sufficiently sampled correlation functions (Zhang et al. 2003a; Doviak et al. (2004)). Within the limits of the considered rms turbulence velocity values, the retrieval uncertainty for a fixed dwell time is smaller for the designed X-band system as compared to the S-band NWRT. It follows that the designed X-band system would require shorter dwell times for fixed retrieval uncertainty as compared to the S-band system. Shorter retrieval times allow for better chances at meeting temporal stationarity.

Third, as the effective decorrelating wind v_s approaches zero, the standard deviation of the G-FCA-retrieved SA baseline wind approaches zero but SZL implementations do not. However, since such scenarios of strict laminar advection of scatterers along the SA baseline rarely, if ever, exist, there is little benefit unique to the usage of the G-FCA.
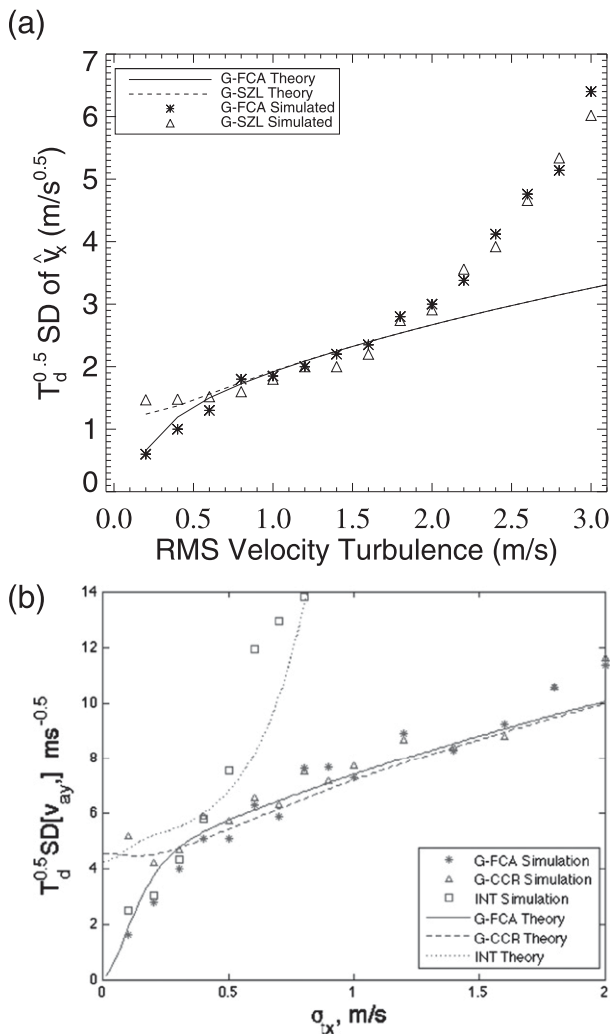
(a)

(b)

(a)

(b)

FIG. 7. (a) The SD of the retrieved SA baseline wind for this study's design vs the rms of turbulence velocity. Parameters as in Table 2. Dwell time $T_d = 10$ s, infinite SNR, along-baseline wind $v_x = 10$ m s^{-1}, and cross-baseline wind $v_y = 0$ m s^{-1}. (b) As in (a), but for the NWRT vs rms turbulence velocity for matched wind speeds, SNR, and dwell time. This figure is reproduced from Li et al. (2009). The label INT refers to the "intercept" retrieval algorithm, which we did not consider because of its known inferior performance.

Figure 8 further shows that the design developed in this study performs well over the indicated range of wind speeds and 10-dB SNR. The slight bias incurred at low wind speeds can be attributed to the effect of the data window. However, since this bias is small relative to wind speed, we see no need to remove the effect of the data window by deconvolution processing.

4. Summary and conclusions

In this work, we have simulated the performance of an X-band spaced antenna radar and investigated the
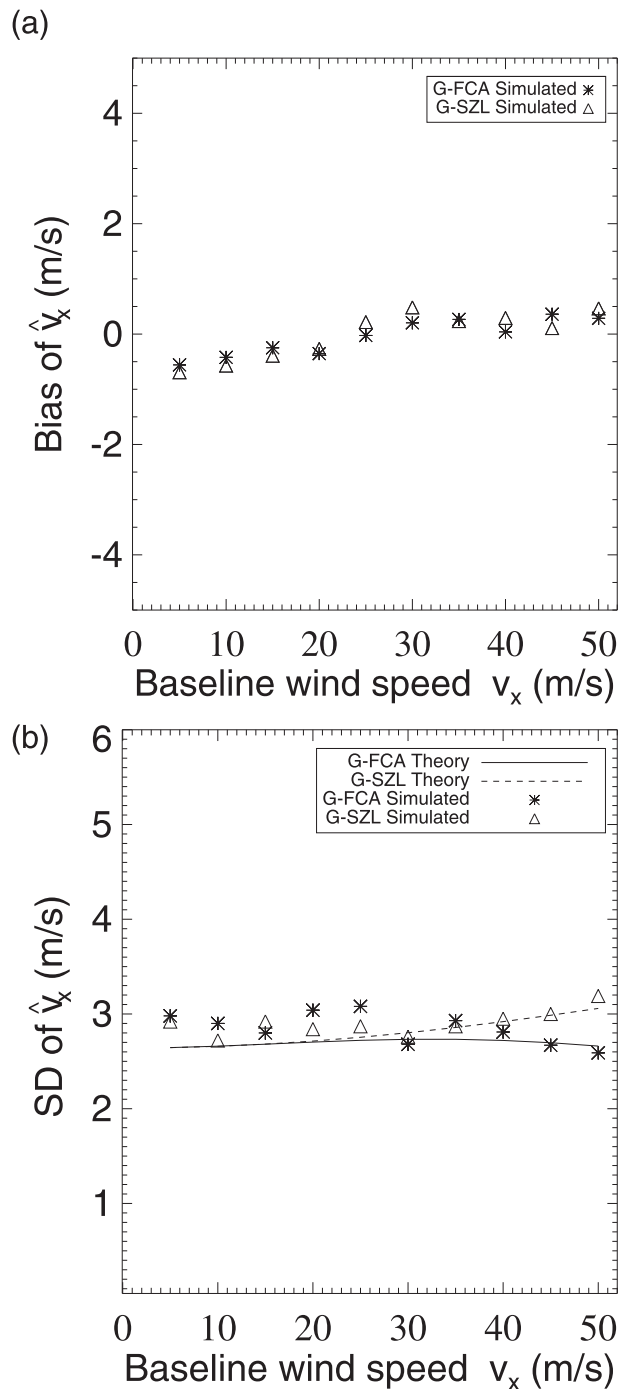
FIG. 8. (a) Bias and (b) SD of retrieved SA baseline wind for this study's design vs SA baseline wind speed assuming 2 m s^{-1} rms turbulence velocity. Parameters as in Table 2, dwell time $T_d = 1$ s, cross-baseline wind $v_y = 0$ m s^{-1}, and a 10-dB SNR.

performance of various retrieval algorithms. Among the investigated algorithms, we find the G-SZL to have the best performance over the investigated design space. It is also simpler, as it obviates the need for noise correction.

TABLE 2. Final X-band phased array spaced antenna design.

PRF	5 kHz
Effective spaced antenna baseline	12 cm
Equivalent one-way antenna azimuthal 3-dB beamwidth	5°

Based on the results of the preceding section, Table 2 outlines the parameters of a candidate X-band spaced antenna phased array radar. To arrive at the design in Table 2, a number of assumptions were implicit, including homogeneity and stationarity of the observed wind within the resolution volume, homogeneity of scatterers in the resolution volume, and the absence of curvature in the mean wind field. The final assumption implies the neglect of the effect of shear within the resolution volume on the baseline wind estimate. It is relevant to mention here that the effect of shear of the radial wind component, if present within the resolution volume, appears to scale with range (Zhang and Doviak 2007; Barrick 1990).

Since spaced antenna retrievals rely on the cross-correlation function expectation, they require longer dwell times than are typically used with scanning weather radars. These dwell times may, however, be accommodated in phased array radar systems with little penalty, as spaced antenna measurements may be interleaved with other types of scans. In some cases, the dwell times required for a particular level of uncertainty may exceed the transit times of scatterers through a resolution volume. In such a case, the signal may become nonstationary.

As a consequence of the shorter wavelength, and hence more rapid decorrelation of the radar echo, the X-band system we consider here appears to promise lower retrieval uncertainty than a system such as the S-band NWRT. However, the rapid decorrelation of the radar echo also limits the ability to sample adequately the spatiotemporal cross-correlation function.

APPENDIX

Equivalence of Slope at Zero-Lag Implementations

In Zhang and Doviak (2007), the cross-correlation function is derived and expressed as a product of Gaussians. Here, we derive a single Gaussian to arrive at the functional forms of retrieval used in Eqs. (5), (10), and (11). Rearranging (1), we get

$$\gamma = e^{-2k^2\sigma_\phi^2 v_x^2\tau^2}e^{-2k^2\sigma_\phi^2\Delta x^2}e^{4k^2\sigma_\phi^2 v_x\tau\Delta x}e^{-2k^2\sigma_\theta^2 v_y^2\tau^2}e^{-2k^2\sigma_{tz}^2\tau^2}.$$
(A1)

Applying the chain rule for differentiation of γ, we see that all terms except the second and third in (A2) vanish

$$\left.\frac{d\gamma}{d\tau}\right|_{\tau=0} = \gamma(\Delta x, 0)4k^2\sigma_\phi^2\Delta x v_x,$$
(A2)

where the second exponent in (A2) that is independent of τ is denoted as $\gamma(\Delta x, 0)$. Because all other terms in (A2) are unity at lag zero, this is always the cross-correlation intercept at zero lag. Note that this depends only on instrumental parameters and is insensitive to meteorological factors.

Denote the product of the remaining four terms that depend on τ as γ_τ,

$$\log_e\gamma_\tau = -2k^2[(\sigma_\phi^2 v_x^2 + \sigma_\theta^2 v_y^2 + \sigma_{tz}^2)\tau^2] - 4k^2\sigma_\phi^2 v_x\tau\Delta x.$$
(A3)

To complete the square, we add and subtract C''^2, such that

$$-2\left(\sqrt{2}k\tau\sqrt{\sigma_\phi^2 v_x^2 + \sigma_\theta^2 v_y^2 + \sigma_{tz}^2}\right)C'' = -4k^2\tau\sigma_\phi^2 v_x\Delta x,$$
(A4)

where

$$C'' = \frac{\sqrt{2}k\sigma_\phi^2 v_x\Delta x}{\sqrt{\sigma_\phi^2 v_x^2 + \sigma_\theta^2 v_y^2 + \sigma_{tz}^2}}.$$
(A5)

Now,

$$\log_e\gamma_\tau = C''^2 + \left[-2k^2\left(\sqrt{\sigma_\phi^2 v_x^2 + \sigma_\theta^2 v_y^2 + \sigma_{tz}^2}\tau - \frac{\sigma_\phi^2 v_x\Delta x}{\sqrt{\sigma_\phi^2 v_x^2 + \sigma_\theta^2 v_y^2 + \sigma_{tz}^2}}\right)^2\right].$$
(A6)

Factoring out the total decorrelating component in the second term,

$$\log_e\gamma_\tau = C''^2 - \left[2k^2(\sigma_\phi^2 v_x^2 + \sigma_\theta^2 v_y^2 + \sigma_{tz}^2)\right.$$
$$\left.\times\left(\tau - \frac{\sigma_\phi^2 v_x\Delta x}{\sigma_\phi^2 v_x^2 + \sigma_\theta^2 v_y^2 + \sigma_{tz}^2}\right)^2\right].$$
(A7)

A rearrangement of terms yields

$$\log_e \gamma_\tau = C''^2 - \left\{ \frac{\left[\tau - \frac{\sigma_\phi^2 v_x \Delta x}{(\sigma_\phi^2 v_x^2 + \sigma_\theta^2 v_y^2 + \sigma_{tz}^2)} \right]^2}{2 \times \frac{1}{4} \times \frac{1}{k^2} \times \frac{1}{\sigma_\phi^2 v_x^2 + \sigma_\theta^2 v_y^2 + \sigma_{tz}^2}} \right\}. \tag{A8}$$

Recognizing that $e^{-\eta} = I_0 e^{C''^2}$ and comparing with (2), it can be shown that

$$\eta = 2k^2 \sigma_\phi^2 \Delta x^2 \frac{v_s^2}{\sigma_\phi^2 v_x^2 + v_s^2}, \tag{A9}$$

$$\tau_p = \sigma_\phi^2 \Delta x \frac{v_x}{\sigma_\phi^2 v_x^2 + v_s^2}, \tag{A10}$$

$$\tau_c = \frac{1}{2k \sqrt{\sigma_\phi^2 v_x^2 + v_s^2}}, \tag{A11}$$

$$v_s^2 = \sigma_\theta^2 v_y^2 + \sigma_{tz}^2, \tag{A12}$$

where $\exp(-\eta)$ is the peak of the cross-correlation coefficient and v_s is an effective decorrelating wind that has contributions from both turbulence velocity and cross-baseline wind (m s^{-1}). Here, τ_p is the time lag to the cross-correlation peak(s) and τ_c is the width of the autocorrelation function(s). These time domain parameters τ_p and τ_c are related to m and σ_w, respectively, in the Doppler domain. Here, m is the slope of the cross-spectral phase with respect to Doppler velocity and σ_w is the Doppler spectrum width (m s^{-1}). Invoking Fourier shift theorem, it can be shown that

$$m = \frac{d}{dv} S(\Delta x, v) = 2k\tau_p. \tag{A13}$$

By the Wiener–Khinchine theorem, we know

$$\sigma_w = \frac{2k}{\tau_c}. \tag{A14}$$

From (A2), (A10), (A11), (A13), and (A14), we see

$$M(\tau = 0) = \frac{d\gamma/d\tau|_{\tau=0}}{\gamma(\Delta x, 0)} = \frac{\tau_p}{\tau_c^2} = \frac{m\sigma_w^2}{2k} = 4k^2 \sigma_\phi^2 \Delta x v_x. \tag{A15}$$

From (A15), it is apparent that the spectral implementation referred to as FSA in this work is equivalent to the slope at zero-lag algorithms G-SZL and D-SZL.

REFERENCES

Barrick, D., 1990: Comment on 'Single station ocean current vector measurement: Application of the spaced antenna (SA) technique.' *Geophys. Res. Lett.,* **17,** 1637–1639.

Briggs, B. H., 1985: The analysis of spaced sensor records by correlation techniques. *Handbook for MAP: Middle Atmosphere Program; Extended Abstracts of Papers Presented at the MAP Symposium, November 26–30, 1984, Kyoto, Japan,* S. Kato, Ed., Vol. 18, University of Illinois at Urbana, 166–186.

——, and R. A. Vincent, 1992: Spaced-antenna analysis in the frequency domain. *Radio Sci.,* **27,** 117–129.

——, G. J. Phillips, and D. H. Shinn, 1950: The analysis of observations on spaced receivers of the fading of radio signals. *Proc. Phys. Soc. London,* **63B,** 106–121.

Caya, D., and I. Zawadski, 1992: VAD analysis of nonlinear wind fields. *J. Atmos. Oceanic Technol.,* **9,** 575–587.

Cheong, B., and R. D. Palmer, 2008: A time-series weather radar simulator based on high-resolution atmospheric models. *J. Atmos. Oceanic Technol.,* **25,** 230–243.

Cohn, S. A., C. L. Holloway, S. P. Oncley, R. J. Doviak, and R. J. Lataitis, 1997: Validation of a UHF spaced antenna wind profiler for high-resolution boundary layer observations. *Radio Sci.,* **32,** 1279–1296.

——, W. O. J. Brown, C. L. Martin, M. E. Susedik, G. D. MacLean, and D. B. Parsons, 2001: Clear air boundary layer spaced antenna wind measurement with the Multiple Antenna Profiler (MAPR). *Ann. Geophys.,* **19,** 845–854.

Doviak, R. J., and D. S. Zrnić, 1993: *Doppler Radar and Weather Observations.* 2nd ed. Academic Press, 562 pp.

——, R. J. Lataitis, and C. L. Holloway, 1996: Cross correlations and cross spectra for spaced antenna wind profilers: 1. Theoretical analysis. *Radio Sci.,* **31,** 157–180.

——, G. Zhang, S. A. Cohn, and W. O. J. Brown, 2004: Comparison of spaced-antenna baseline wind estimators: Theoretical and simulated results. *Radio Sci.,* **39,** RS1006, doi:10.1029/2003RS002931.

Hardwick, K.-M., S. J. Frasier, A. L. Pazmany, H. B. Bluestein, and M. M. French, 2005: Spaced antenna measurements of cross beam velocity in severe storms. Preprints, *32nd Conf. on Radar Meteorology,* Albuquerque, NM, Amer. Meteor. Soc., P4R.11. [Available online at https://ams.confex.com/ams/32Rad11Meso/techprogram/paper_96273.htm.]

Holdsworth, D., and I. M. Reid, 1995a: A simple model of atmospheric radar backscatter: Description and application to the full correlation analysis of spaced-antenna data. *Radio Sci.,* **30,** 1263–1280.

——, and ——, 1995b: Spaced-antenna analysis of atmospheric radar backscatter model data. *Radio Sci.,* **30,** 1417–1433.

Holloway, C. L., R. J. Doviak, S. A. Cohn, R. J. Lataitis, and J. S. V. Baelen, 1997: Cross correlations and cross spectra for spaced antenna wind profilers. 2: Algorithms to estimate wind and turbulence. *Radio Sci.,* **32,** 967–982.

Kramar, M., H. B. Bluestein, A. L. Pazmany, and J. D. Tuttle, 2005: The "Owl Horn" signature in developing southern plains supercells. *Mon. Wea. Rev.,* **133,** 2608–2634.

Kudeki, E., and F. Sürücü, 1991: Radar interferometric imaging of field-aligned plasma irregularities in the equatorial electrojet. *Geophys. Res. Lett.,* **18,** 41–44.

Larsen, M. F., and J. Röttger, 1989: The spaced antenna technique for radar wind profiling. *J. Atmos. Oceanic Technol.,* **6,** 920–938.

Lataitis, R. J., S. F. Clifford, and C. L. Holloway, 1995: An alternate method for inferring winds from spaced-antenna radar measurements. *Radio Sci.,* **30,** 463–474.

Lhermitte, R., and D. Atlas, 1961: Precipitation motion by pulse Doppler radar. Preprints, *Ninth Weather Radar Conf.,* Kansas City, MO, Amer. Meteor. Soc., 218–223.

Li, Y., R. J. Doviak, and G. Zhang, 2009: Spaced antenna interferometric measurements of crossbeam wind using a Monte Carlo simulator based on the configuration of the NWRT. Preprints, *34th Conf. on Radar Meteorology,* Williamsburg, VA, Amer. Meteor. Soc., P12.5. [Available online at https://ams.confex.com/ams/34Radar/techprogram/paper_156107.htm.]

Muschinski, A., 2004: Local and global statistics of clear-air Doppler radar signals. *Radio Sci.,* **39,** RS1008, doi:10.1029/2003RS002908.

Pazmany, A., H. B. Bluestein, M. M. French, and S. Frasier, 2004: Observations of the two-dimensional wind field in severe convective storms using a mobile, X-band, Doppler radar with a spaced antenna. Preprints, *22nd Conf. on Severe Local Storms,* Hyannis, MA, Amer. Meteor. Soc., P7.3. [Available online at https://ams.confex.com/ams/11aram22sls/techprogram/paper_81118.htm.]

Probert-Jones, J., 1960: Meteorological use of pulse Doppler radar. *Nature,* **186,** 271–273.

Rinehart, R., and E. Garvey, 1978: Three-dimensional storm motion detection by conventional weather radar. *Nature,* **273,** 287–289.

Salazar, J. L., R. Medina, E. J. Knapp, and D. J. McLaughlin, 2008: Phase-tilt array antenna design for dense distributed radar network for weather sensing. *2008 IEEE International Geoscience and Remote Sensing Symposium: Proceedings,* Vol. 5, IEEE, V-318–V-321.

Shapiro, A., P. Robinson, J. Wurman, and J. Gao, 2006: Single-Doppler velocity retrieval with rapid-scan radar data. *J. Atmos. Oceanic Technol.,* **20,** 1758–1777.

Smythe, G., and D. S. Zrnić, 1983: Correlation analysis of Doppler radar data and retrieval of the horizontal wind. *J. Climate Appl. Meteor.,* **22,** 297–311.

Sroga, J. T., E. Eloranta, and T. Barber, 1980: Lidar measurement of wind vertical velocity profiles in the boundary layer. *J. Appl. Meteor.,* **19,** 598–605.

Zhang, G., and R. J. Doviak, 2007: Spaced-antenna interferometry to measure crossbeam wind, shear and turbulence: Theory and formulation. *J. Atmos. Oceanic Technol.,* **24,** 791–805.

——, ——, J. Vivekanandan, W. O. J. Brown, and S. A. Cohn, 2003a: Cross-correlation ratio method to estimate cross-beam wind and comparison with a full correlation analysis. *Radio Sci.,* **38,** 8052, doi:10.1029/2002RS002682.

——, ——, and T.-Y. Yu, 2003b: Angular and range interferometry to measure wind. *Radio Sci.,* **38,** 1106, doi:10.1029/2003RS002927.

——, ——, ——, W. O. J. Brown, and S. A. Cohn, 2004: Performance of correlation estimators for spaced-antenna wind measurement in the presence of noise. *Radio Sci.,* **39,** RS3017, doi:10.1029/2003RS003022.